Published in final edited form as:
Biochemistry. 2010 March 23; 49(11): 2491–2501. doi:10.1021/bi902135e.

Structural analysis and functional implications of the negative mTORC1 regulator REDD1

Silvia Vega-Rubin-de-Celis[‡,§,Ψ], **Zeina Abdallah**[‖], **Lisa Kinch**[⊥], **Nick V. Grishin**[⊥], **James Brugarolas**[‡,§,Ψ,*], and **Xuewu Zhang**[‖,⊥,*]

[‡] Department of Developmental Biology, University of Texas Southwestern Medical Center, Dallas, TX, 75390, USA

[§] Simmons Comprehensive Cancer Center, University of Texas Southwestern Medical Center, Dallas, TX, 75390, USA

[Ψ] Department of Internal Medicine, Oncology Division, University of Texas Southwestern Medical Center, Dallas, TX, 75390, USA

[‖] Department of Pharmacology, University of Texas Southwestern Medical Center, Dallas, TX, 75390, USA

[⊥] Department of Biochemistry, University of Texas Southwestern Medical Center, Dallas, TX, 75390, USA

Abstract

REDD1 is a conserved stress-response protein that regulates mTORC1, a critical regulator of cell growth and proliferation that is implicated in cancer. REDD1 is induced by hypoxia and REDD1 overexpression is sufficient to inhibit mTORC1. mTORC1 is regulated by the small GTPase Rheb, which in turn is regulated by the GTPase-activating protein complex, TSC1/TSC2. REDD1 induced-mTORC1 inhibition requires the TSC1/TSC2 complex, and REDD1 has been proposed to act by directly binding to and sequestering 14-3-3 proteins away from TSC2 leading to TSC2-depedent inhibition of mTORC1. Structure/function analyses have led us to identify two segments in REDD1 that are essential for function, which act in an interdependent manner. We have determined a crystal structure of REDD1 at 2.0 Å resolution, which shows that these two segments fold together to form an intact domain with a novel fold. This domain is characterized by an α/β sandwich consisting of two antiparallel α-helices and a mixed β-sheet encompassing an uncommon psi-loop motif. Structure-based docking and functional analyses suggest that REDD1 does not directly bind to 14-3-3 proteins. Sequence conservation mapping to the surface of the structure and mutagenesis studies demarcated a hotspot likely to interact with effector proteins that is essential for REDD1-mediated mTORC1 inhibition.

Keywords

REDD1; DDIT4; 14-3-3; Hypoxia; mTOR; TSC2

[*]Corresponding author James.Brugarolas@UTSouthwestern.edu Phone: 214-648-4099; Fax: 214-648-1960 Xuewu.Zhang@UTSouthwestern.edu Phone: 214-645-6116; Fax: 214-645-6138.

[††]The coordinates of the crystal structure of REDD1 have been deposited in the PDB with the PDB ID 3LQ9.

Supporting information is available, including supplemental results and five supplemental figures, free of charge via Internet at http://pubs.acs.org/journal/bichaw.

mTORC1 (mammalian target of rapamycin complex 1) is a protein complex that plays an important role in the regulation of anabolic processes and cell growth. The best characterized function of mTORC1 is in promoting protein synthesis. mTORC1 promotes mRNA translation initiation, at least in part, by facilitating the assembly of a preinitiation complex at the 5' end of nuclear-encoded mRNAs (at a m^7GTP moiety referred to as the cap) (1). mTORC1 is composed of a core complex consisting of two subunits, the atypical protein kinase mTOR (mammalian target of rapamycin), and the adaptor protein raptor (regulatory-associated protein of mTOR) (2,3). Several additional mTORC1 partners have been described including mLST8 (mammalian lethal with Sec13 protein 8) (4,5), which at least during development appears to be dispensable for mTORC1 function (6), PRAS40 (proline-rich Akt substrate of 40 kDa) (7,8) and DEPTOR (DEP domain TOR binding protein) (9). mTORC1 phosphorylates 4E-BP1 (eukaryotic initiation factor 4E [eIF4E]-binding protein 1) releasing it thereby from eIF4E at the 5' cap and allowing eIF4E interaction with eIF4G and the nucleation of a preinitiation complex (1). mTORC1 also phosphorylates S6K1 (S6 kinase 1), and this phosphorylation event [at Thr^{389}; (10)] primes S6K1 for further phosphorylation and activation. S6K1 in turn phosphorylates, among others, eIF4B, a component of the preinitiation complex, and the small ribosomal subunit protein S6 (11).

mTORC1 activity is tightly regulated by a variety of cues including the availability of nutrients and energy resources as well as oxygen and growth factors (12). mTORC1 interacts with the small G protein Rheb (Ras homologue enriched in brain) (13), and in vitro, GTP-loaded Rheb has been shown to activate mTORC1 (7). The levels of Rheb·GTP are in turn regulated by a protein complex with GAP (GTPase-activating protein) activity formed by the proteins tuberous sclerosis complex 1 (TSC1) and 2 (TSC2). The TSC1/TSC2 complex, and in particular TSC2 is extensively phosphorylated in response to upstream signals and these phosphorylation events play a very important role in the relay of signals to mTORC1 (11). Among other kinases, TSC2 is phosphorylated in response to growth factors by Akt (14-16), and Akt phosphorylation is thought to result in TSC2 binding to 14-3-3 (17), a process that may be important for TSC2 inactivation and consequent activation of mTORC1 (18).

Oxygen signals are relayed to mTORC1 through a process that involves REDD1 (regulated in development and DNA damage response 1; also called DDIT4). REDD1 is a 25 kDa protein that is transcriptionally upregulated in response to hypoxia (19). REDD1 is necessary for hypoxia-induced mTORC1 inhibition in fibroblasts and REDD1 overexpression is sufficient to inhibit mTORC1 (20). In addition, other stress conditions upregulate REDD1 (21), including ER stress (22) and DNA damage (23). The inhibition of mTORC1 by REDD1, or its paralogue REDD2 (also called DDIT4L), requires the TSC1/TSC2 complex (20) and can be blocked by Rheb (24,25). It has been reported that in response to hypoxia, TSC2 dissociates from 14-3-3 proteins and REDD1 overexpression appeared to similarly disrupt TSC2 binding to 14-3-3 (26). While TSC2 binding to 14-3-3 is thought to be phosphorylation dependent, TSC2 phosphorylation at 14-3-3 binding sites appeared to be unaffected by hypoxia (26). It has been proposed that REDD1 acts by directly binding to 14-3-3 proteins and sequestering them away from TSC2 leading thereby to TSC2 activation (26). A putative 14-3-3 binding site was identified in REDD1 whose disruption impaired REDD1 function, and REDD1 was found to interact with 14-3-3 proteins in overexpression studies in cell lysates.

Here we report the crystal structure of REDD1 and evaluate its functional implications in the context of the reported model for REDD1 action.

EXPERIMENTAL PROCEDURES

Reagents

Antibodies were obtained from the following sources: Covance, HA.11; Invitrogen, V5; Sigma, α−tubulin (clone B-5-1-2) and FoxO3; Cell Signaling: phosphorylated S6K1 (T389), phosphorylated S6 (S235/S236), S6, S6K1, eIF4E, 4E-BP1 and GST antibodies; Bethyl: HIF1α, TSC1 and REDD1; Santa Cruz: TSC2, HA (Y-11), REDD1 (N-20) and normal mouse IgG; Biosource, PRAS40; Lab Vision, pan-14-3-3. The REDD1 monoclonal antibody was described (Kucejova et al., submitted). The following were gifts: pRK7-HA-S6K (rat αII isoform) (J Blenis, Harvard Medical School), pcDNA3-Flag-Rheb (B Manning, Harvard School of Public Health), pDONR223-REDD1 (human) (M. Vidal, Dana-Farber Cancer Institute). pRK5-Flag-PRAS40 plasmid was obtained from Addgene. siRNA oligonucleotides for TSC2 (20) and REDD1 (27) were purchased from Dharmacon. HRP-conjugated secondary antibodies were purchased from the following sources: Pierce, goat anti rabbit IgG and goat anti-mouse IgG; Jackson Immunolabs, goat anti-mouse IgG light chain; Santa Cruz, donkey anti-goat IgG. TnT Quick Coupled transcription-translation kit was purchased from Promega and used according to manufacturer's instructions.

Cloning and mutagenesis

Plasmids were generated by site-directed mutagenesis (Quikchange mutagenesis kit, Stratagene) according to manufacturer's instructions with minor modifications or by PCR of human REDD1 cDNA in pcDNA3 (20). All cDNAs were validated by sequencing. Plasmids (Database ID): HA-REDD1 N-terminal deletion series [48-232 (#182), 77-232 (#426), 85-232 (#427), 101-232 (#183)]; C-terminal deletion series [1-165 (#187), 1-192 (#421), 1-209 (#430), 1-225 (#431)]; internal deletions [Δ96-157 (#188), Δ96-110 (#189), Δ111-135 (#190), Δ136-153 (#191), Δ200-204 (#597)]; “NAAIRS” substitutions [N109-119 (#432), N132-145 (#433), N153-165 (#434), N166-178 (#435), N179-193 (#437), N194-206 (#436), N207-225 (#439), N181-211 (#595), N187-207 (#596)]; point mutations [S103W (#623), S103L (#624), R133A (#564), S137A (#627), S137D (#628), P139A (#625), R133A/P139A (#626), C140S (#622), C150S (#516), C157S (#517), K219A (#565), L221A (#567), Y222A (#566), K219A/Y222A (#568)]. V5-REDD1 (#272B) was shuttled from pDONR223-REDD1 using the Gateway cloning system (Invitrogen) to a pDEST3.2 vector. *REDD1*$^{85\text{-}193}$ (#465) and *REDD1*$^{207\text{-}225}$ (#442) expression constructs were cloned in a pCMV-GST vector.

For REDD1 crystallization the human REDD1 cDNA sequence coding for amino acids 89-226 was amplified by PCR and cloned using BamHI and XhoI sites into a modified pET28 vector (Novagen) expressing the target protein with an N-terminal His_6-Sumo tag. The mutant with residues 200-204 deleted was generated by Quikchange reaction (Stratagene). Expression vectors were transformed into the bacteria strain BL21(DE3) and protein expression was induced in TB medium with 0.5 mM IPTG at 18 °C overnight. Seleno-methionine replaced protein was expressed in the same bacteria strain by using the protocol described elsewhere (28). The protein was first purified using a 1 ml HisTrap column (GE Healthcare). The N-terminal His_6-Sumo tag was then removed by treatment by a Sumo-specific protease Ulp1 at 4 °C overnight. The protein was further purified by a UnoS cation exchange column (Bio-Rad), concentrated to ~10 mg/ml and stored at −80 °C.

Crystallization, structure determination and refinement

Crystals of both native and selenomethionine replaced protein were grown in 0.1 M NaF, 20-26% PEG3350, and 0.05 mM $C_{12}E_9$ (polyoxyethelene-9-lauryl ether, Hampton Research) in 4 °C. Diffraction data were collected at the beamline 19BM at the advanced photon source (Argonne, IL). The structure was solved by selenomethionine single-

wavelength anomalous dispersion (SAD) using the program suite Phenix. The initial SAD electron density map was of sufficient quality and a partial model was built by the Autobuild module in Phenix (29). Subsequent iterative manual model building and refinement were performed using the programs Coot and Phenix, respectively (30). Statistics for data collection and refinement are summarized in Table 1. The sequence alignment and similarity scores were calculated using the program Clustal X (31). All the molecular graphics were rendered in Pymol (http://www.pymol.org).

Tissue culture

HeLa cells and MEFs were grown at 21% O_2 and 5% CO_2 in a humidified incubator in high glucose DMEM (Dubelcco) supplemented with 10% heat-inactivated fetal bovine serum (Atlanta Biologicals) and 1% Penicillin/Streptomycin (Gibco). U2OS HA-REDD1 cells were grown under similar conditions with Puromycin (1 μg/ml) and Hygromycin (50 μg/ml) and induction was performed with 1 μg/ml tetracycline (Sigma) for 3 hours unless otherwise specified. Cells were exposed to hypoxia conditions (1% O_2, 5% CO_2) for 3 hours in a hypoxia chamber (Coy Laboratory Products).

Transfections

Plasmid DNA was transfected using the MirusIT-LT1 transfection reagent (Mirus BioCorporation) according to the manufacturer's recommendations. The relative amounts of expression vector DNA to be transfected were adjusted (when necessary) to obtain similar protein levels and the amount of transfected DNA was kept the same in all reactions by supplementing transfection mixtures with the corresponding empty vector. Cells were harvested 48 hours after transfection. siRNA oligonucleotides were transfected with Oligofectamine (Invitrogen) according to manufacturer's instructions and cells were harvested 48 hours after transfection.

Cell lysates and western blot

Cells were washed with PBS and lysed in lysis buffer [50 mM Tris-HCl (pH 7.4), 250 mM NaCl, 0.5% Igepal] supplemented with protease inhibitors [0.1 μM aprotinin (USB), 0.02 mM leupeptin (USB), 0.01 mM pepstatin (USB), 0.5 mM benzamidine (Sigma), 0.5 mM PMSF (Sigma), 0.01 M NaF (Sigma)] and phosphatase inhibitors [2 mM imidazole (Sigma), 1.15 mM sodium molybdate (Sigma), 1 mM sodium orthovanadate (Sigma), 5 nM microcystin (Calbiochem)] for 10 minutes at 4°C. Lysates were cleared by centrifugation at 16000 g for 10 minutes, and protein concentration was measured by Bradford's method (BioRad). Protein lysates were supplemented with 3x SDS-loading buffer (6.7% SDS, 33.3% glycerol, 300 mM DTT, bromophenol blue) and denatured by boiling for 10 minutes. Similar amounts of protein were resolved by SDS-PAGE, transferred to a nitrocellulose membrane (BioRad), blocked with 5% milk in TBST (10 mM Tris-HCl, 15 mM NaCl, 0.1% Tween-20) and probed for the desired primary antibodies followed by appropriate secondary antibodies conjugated to HRP and the signal was detected by chemiluminiscence [mixing 1:1 solution 1 (2.5 mM luminol, 0.4 mM pCoumaric acid, 0.1 M Tris-HCl) and solution 2 (0.015% H_2O_2, 0.1 M Tris-HCl)].

Immunoprecipitations

Cells were rinsed with ice-cold PBS twice and lysed with IP buffer [50 mM Tris-HCl (pH 7.4), 150 mM NaCl, 0.5% Igepal)] supplemented with protease and phosphatase inhibitors for 10 minutes at 4°C. Cell lysates were cleared by centrifugation at 16000 g for 10 minutes, and pre-cleared with protein A (or protein G) sepharose beads (Amersham; 50% slurry in IP buffer) for 1 hour at 4°C. Samples were normalized for protein content and rocked in the presence of ~1 μg of antibody/mg of protein overnight at 4°C. Protein A or protein G

sepharose was added for 1 hour at 4°C and immunoprecipitates were recovered by centrifugation. After washing with IP buffer 3 times, 1x loading buffer was added, samples were boiled, resolved by SDS-PAGE and evaluated by western blot.

m^7GTP affinity chromatography

Cells were washed with ice-cold PBS and lysed in IP buffer containing protease and phosphatase inhibitors. Cell lysates were cleared by centrifugation and incubated with m^7GTP sepharose beads (Amersham; 50% in IP buffer) for 2 hours at 4°C. Beads were recovered by centrifugation, washed 3 times with IP buffer, resuspended in 1x loading buffer, and protein was eluted by boiling in SDS loading buffer. Protein samples were resolved by SDS-PAGE and evaluated by western blot.

Sequence alignment and phylogenetic tree

REDD1 sequences were collected using PSI-BLAST (32) and aligned with PROMALS-3D (33). Distances were calculated from the alignment using an amino acid transition probability matrix (34). Initial tree topologies were built using the Njdist program of the MOLPHY package (35,36). Maximum likelihood trees were built using a local rearrangement search of tree topology (-R option) of PROTML (35). The reliability of the resulting tree topologies were assessed by the resampling of estimated log-likelihood method of MOLPHY (37).

RESULTS

Structure/function analyses of REDD1

The REDD proteins (REDD1 and REDD2) arose through a gene duplication event that occurred independently in humans and insects (see Figure S1 in the supplemental material) and regulate mTORC1 in response to different stimuli (21). REDD1 is induced by hypoxia (Figure 1A), and REDD1 overexpression is sufficient to inhibit mTORC1 (Figure 1B-D). mTORC1 inhibition by REDD1 requires the TSC1/TSC2 complex (Figure 1E), but REDD1 does not appear to interact with TSC1/TSC2; in reciprocal immunoprecipitation experiments, and under conditions in which TSC1 was recovered bound to TSC2, REDD1 was not found in the complex (Figure 1F). REDD1-induced mTORC1 inhibition can also be blocked by overexpression of Rheb (Figure 1G).

To obtain insight into the mechanism of REDD1 action, structure/function analyses were performed in HeLa cervical carcinoma cells, a cell type in which (1) hypoxia results in a REDD1-dependent inhibition of mTORC1 (Figure 1H), and (2) *REDD1* overexpression is sufficient to inhibit mTORC1 (Figure 2A). *REDD1* mutants were transfected into HeLa cells along with an expression vector for the p70 isoform of S6K1 that would serve as a readout. Consistent with sequence conservation studies, which revealed that the N-terminus of REDD1 was poorly preserved, the N-terminal 84 amino acids of REDD1 were dispensable for function (Figure 2A). However, deletion into a sequence predicted to form a α helix (beyond Glu^{90}) disrupted REDD1 activity (Figure 2A). In contrast, the C-terminus of REDD1 is well conserved and only a few residues could be deleted without disrupting function (Figure 2B). Internal deletions were poorly tolerated (Figures 2C). Because internal deletion may disrupt the structure by juxtaposing residues that force the protein into an unphysiological conformation, experiments were also conducted using a flexible linker previously shown to be able to adopt both a α-helix or a β-strand conformation (NAAIRS, single amino acid code; (38)). As for internal deletions, NAAIRS substitutions were poorly tolerated (Figures 2D-E). In one instance, however, a NAAIRS substitution was tolerated encompassing a poorly conserved region predicted not to adopt any secondary structure ($REDD1^{194\text{-}206}$; Figure 2D). These data indicated that there were two linear segments in the

REDD1 sequence required for function (REDD1$^{85\text{-}193}$ and REDD1$^{207\text{-}225}$) separated by a dispensable region (Figure S2).

To determine whether the isolated segments, REDD1$^{85\text{-}193}$ and REDD1$^{207\text{-}225}$, retained some functionality, their ability to act as dominant negative (i.e., inhibit wild-type REDD1) was individually evaluated. Hemmaglutinin (HA)-tagged versions of *REDD1$^{85\text{-}193}$* and *REDD1$^{207\text{-}225}$* were subcloned into a *GST* expression vector and transfected into HA-REDD1-inducible cells. Expression of REDD1$^{85\text{-}193}$ or REDD1$^{207\text{-}225}$ at levels higher than full length inducible REDD1 failed to block wild-type REDD1 function (Figure 2F, G). These data indicate that REDD1$^{85\text{-}193}$ and REDD1$^{207\text{-}225}$ do not function as dominant negative, suggesting that neither of the two functionally important regions when expressed separately is able to interact with (and titrate out) binding partners of REDD1 required for its function.

REDD1 crystal structure reveals a novel topology

Failure of REDD1$^{85\text{-}193}$ and REDD1$^{207\text{-}225}$ to act as dominant negative suggests that they function in an interdependent manner. To explore this possibility further and to obtain additional insight into the molecular mechanism of REDD1 action we sought to solve its crystal structure. Based on the functional studies above and secondary structure predictions, we decided to crystallize a segment of human REDD1 encompassing amino acids 89-226, which preserves the putative N-terminus α helix and all essential C-terminal residues. REDD1$^{89\text{-}226}$ was prone to precipitation, however, and despite extensive attempts it did not crystallize. An assessment of factors contributing to the lack of solubility led to the discovery of a hydrophobic region (^{200}FLPGF^{204}) which was absent in orthologues in other species, such as *Drosophila* (Figure S3), which have been previously shown to similarly inhibit dTor (39). This hydrophobic stretch corresponded to a region between the two essential REDD1 segments that was predicted to be unstructured and could be substituted for a NAAIRS sequence without affecting function (Figure 2D). In addition, simply deleting ^{200}FLPGF^{204} did not affect REDD1 activity (Figure 2E). REDD1$^{89\text{-}226}$ with a deletion of ^{200}FLPGF^{204} (REDD1$^{89\text{-}226\Delta\phi}$) was more soluble and yielded crystals that diffracted beyond 2.0 Å resolution.

The overall structure of REDD1 is characterized by a two-layered sandwich with one layer made strands ordered 2134 (Figure 3B). Strands β1-β3 form a rare structural motif known as a psi-loop, two antiparallel strands separated by an intervening strand that makes hydrogen bonds with both flanking strands (40). Of note, residues flanking the ^{200}FLPGF^{204} deletion formed a loop that, as predicted, did not adopt any secondary structure. In keeping with the idea that the deletion does not impose any restrains on the structure, this loop represented the most flexible region in REDD1$^{89\text{-}226\Delta\phi}$ (highest B-factors). There were two REDD1$^{89\text{-}226\Delta\phi}$ molecules (A and B) in the unit cell of the P1 space group, which were essentially identical to each other; these two proteins did not, however, form a symmetric dimer and no evidence for dimerization was observed by gel filtration chromatography of the purified protein (Figure 3C). In addition, REDD1 did not appear to oligomerize in cells as determined by immunoprecipitation experiments of cells expressing REDD1 fused to two different epitope tags (Figure 3D).

At a glance the topology of REDD1 seemed unusual. To determine whether other proteins existed with a similar topology, structure searches were conducted on the PDB (Protein data bank, www.pdb.org). A PDB search using Dali (41) did not reveal any significant hits (Z-score > 5). The top Dali hit (Z-score 3.8) was a structure with two similar antiparallel α-helices packed against a β-sheet (PDB ID: 1i2l). However, the β-strands were ordered differently and the structure lacked the psi-loop motif (compare Figure 4B with 4A). A less stringent structure topology search using ProSMoS (42) identified a portion of the YrdC-like

hypothetical protein (PDB ID: 1K7J) as a top hit (Figure 4C). Although the identified YrdC-like region includes two antiparallel α-helices packed against a β-sheet of similar strand order to REDD1, the cross connecting "loop" of the psi-loop motif forms the main structural core of the protein. Inspection of evolutionarily related YrdC-like structures classified by the database SCOP (Structure classification of proteins) (43) revealed that the identified YrdC-like substructure was not conserved and that it was unlikely to form independently of the core, and thus it was unlikely to be related to REDD1. Two other candidates identified by the ProSMoS topology search were representative structures of two all-β class families: a pua domain-like pseudobarrel (PDB ID: 3d79) and a Lexa-related family C-terminal domain (PDB ID: 2fjr). While these hits contained the unusual psi-loop motif, their overall topology was unrelated to REDD1 (Figure 4D, E). Taken together these data show that the topology of REDD1 is unique.

Conservation and mutagenesis studies define a surface patch on REDD1 critical for function

The uniqueness of REDD1 structure precluded inferences about structure/function relationships. Mapping of REDD1 sequence conservation to the crystal structure revealed a surface patch composed of highly conserved residues (Figure 5A and B) formed largely by two segments that are not contiguous in the primary sequence but cluster together in the three-dimensional structure. The first stretch was made up by a loop between helix α2 and strand β1 (^{138}EPCG^{141}) and the second by the C-terminal portion of strand β4 (^{218}KKKLYSSE^{225}) (Figure 5A). To evaluate the functional significance of this conserved surface patch, single amino acid substitutions were introduced. A conservative substitution of Cys^{140} by a serine residue mildly impaired REDD1 function (Figure S4B). In addition, individual mutation of Lys^{219}, Leu^{221} and Tyr^{222} to alanine residues resulted in similarly modest functional impairments (Figures 5C and D). However, simultaneous alanine substitutions of Lys^{219} and Tyr^{222} completely abrogated REDD1 function (Figure 5D). Since all of the mutated residues are surface exposed and do not make structurally significant interactions, it is unlikely that the effects of these mutations are due to destabilization of the REDD1 structure. Thus, these results suggest that this conserved surface patch is a functional hotspot likely responsible for interacting with binding partners and essential for signaling.

We observed in the REDD1 structure a large hydrophobic pocket located between helix α1 and strand β2. In the crystal, this pocket accommodated a leucine residue (Leu^{192}) from the second REDD1 molecule (molecule B; Figure S4A). We found that residues forming the base were conserved (Leu^{96}, Leu^{100}, Leu^{104}, Leu^{147}, Val^{149} and Val^{160}) but those forming the ridge were not. Substitutions intended to block access to the pocket (S103L and S103W) did not however appreciably affect REDD1 function (Figure S4B).

Functional implications of REDD1 structure with respect to 14-3-3 binding model

REDD1 was proposed to act by directly interacting with 14-3-3 proteins through ^{133}RLAYSEP^{139}, a sequence that conforms to a putative 14-3-3 binding motif (26). Canonical binding to 14-3-3 proteins typically involves an unstructured motif including a phosphorylated serine residue, which largely determines the binding affinity and specificity by interacting with a positively charged patch in the ligand-binding groove of 14-3-3 proteins (44). The serine residue is typically preceded by an arginine at position -3 (mode I) or -4 (mode II) and followed by a proline at position +2 (45,46). The ^{133}RLAYSEP^{139} motif conforms to a mode II 14-3-3 binding peptide, which typically interact in a largely linear conformation. However, the ^{133}RLAYSEP^{139} motif in the REDD1 structure forms part of helix α2 and the subsequent loop (Figure 6A). Binding of this segment to 14-3-3 would require a dramatic conformational change with at least partial unfolding of helix α2, and this

would be predicted to destabilize the structure and is therefore unlikely to occur. Furthermore, while phosphorylation of the conserved serine residue in mode II peptides plays a critical role in stabilizing their interaction with 14-3-3 proteins (46), Ser^{137} in REDD1 is not well conserved (Figure S3) and Ser^{137} mutation to alanine does not affect REDD1 function (Figure 6C).

While most proteins bind to 14-3-3 proteins through a linear peptide motif, Exoenzyme S interacts with 14-3-3β through a motif in a α helical conformation (Figure 6B and (44)). In this instance, the helical structure lies in the 14-3-3 substrate-binding groove in the opposite orientation of mode I and II peptides. We attempted manually docking REDD1 onto 14-3-3β based on this binding mode by superimposing the helical portion of the binding motif in REDD1 onto the Exoenzyme S peptide. REDD1 could not be docked without many inevitable steric clashes (Figure 6B). The narrow substrate-binding groove in 14-3-3 was not able to accommodate the neighboring α1 helix and β4 strand. In addition, the potential binding motif in REDD1 did not show the amphipathic property of the exoenzyme S peptide that established binding specificity for 14-3-3 (Figure 6B). These observations strongly suggest that REDD1 does not bind to 14-3-3 in this rare helical mode either.

We find that simultaneous mutation of Arg^{133} and Pro^{139} to alanine residues, as previously shown (26), disrupts REDD1 function (Figure 6C), but mutation of Pro^{139} alone is sufficient for this effect (Figure 6C). Notably, Pro^{139} is also part of the conserved surface patch and that may explain its importance for REDD1 function (Figure 5A).

By gel filtration studies, purified $REDD1^{89\text{-}226\Delta\phi}$ did not interact with 14-3-3β (Figure 7A). Similarly in vivo experiments failed to show an interaction between REDD1 and 14-3-3 proteins. Under conditions in which 14-3-3 proteins were found to bind known interacting partners like PRAS40 (47) and FoxO3 (Forkhead box O3; (48)), we could not detect binding of endogenous 14-3-3 proteins to REDD1 (either overexpressed or endogenous) using a variety of experimental systems (Figures 7B, C and S5A, B). These data suggest that REDD1 does not interact with 14-3-3 proteins directly (or perhaps even indirectly). While REDD1 induction appeared to decrease the amount of TSC2 bound to 14-3-3 in pan-14-3-3 immunoprecipitations, the significance of these findings remains to be fully elucidated and REDD1 was not found to bind to 14-3-3 (Figure 7D and E).

DISCUSSION

Herein we report structure/function analyses of the REDD1 protein, a protein that plays a critical role in the regulation of mTORC1 in response to stress. The crystal structure of the C-terminal functional domain of REDD1 shows a novel topology consisting of an independently folded α/β sandwich with a psi-loop motif. We have identified a conserved surface patch formed primarily by the carboxy-terminal end of strand β4 and the loop between helix α2 and strand β1 as a functional hotspot that is essential for REDD1 signaling.

It was previously proposed that REDD1 functions by directly interacting with and sequestering 14-3-3 proteins from TSC2 (26). Several lines of evidence suggest that this model may not be correct. First, the alleged 14-3-3 binding motif in REDD1 (^{133}RLAYSEP^{139}) is not conserved (Figure 5B); and Arg^{133} and Ser^{137} in the motif, which are key determinants for 14-3-3 binding, are replaced by other residues in orthologues in *Xenopus* and *Drosophila*, respectively (Figure S3). Second, mutation of either Ser^{137} or Arg^{133} does not affect REDD1-induced inhibition of mTORC1 (Figure 6C). Third, the REDD1 structure does not conform to any mode known of 14-3-3 interaction (Figure 6A, B). Fourth, no evidence for interaction was observed in vitro (Figure 7A), or in vivo when endogenous proteins were evaluated and under conditions in which binding of 14-3-3

proteins to other interacting proteins was appreciated (Figure 7B and C). Fifth, the finding that mutations in Pro^{139} disrupt function may be explained by its forming part of the conserved surface hotspot we identified (rather than by disrupting binding to 14-3-3 proteins directly) (Figure 5A). Finally, given that 14-3-3 proteins are rather abundant and are involved in interacting with over 70 proteins in cells (49), it is not clear how they would be sequestered effectively and specifically from TSC2 by REDD1 under hypoxia. Taken together these data strongly suggest that REDD1 does not function by directly interacting with 14-3-3 proteins.

REDD1-induced mTORC1 inhibition requires the TSC1/TSC2 complex, but REDD1 does not appear to interact with TSC1/TSC2. While proteins that interact with REDD1 and relay signals to TSC1/TSC2 remain to be identified, the functional hotspot in REDD1 is likely the binding site for these proteins. The crystal structure will allow us to design mutations that specifically disrupt this hotspot without affecting the overall structure of REDD1, which will prove to be valuable in distinguishing authentic and nonspecific hits in futures efforts on identifying REDD1 binding proteins.

Another potentially interesting site that emerged from analyses of the structure was a large hydrophobic pocket located between helix α1 and strand β2. In the crystal, this pocket in one molecule (molecule A) accommodated a leucine residue (Leu^{192}) from the second REDD1 molecule (molecule B; Figure S4A). However, this pocket in molecule B did not make such an interaction and gel filtration chromatography of the purified protein failed to show evidence for oligomerization. In addition, REDD1 did not seem to oligomerize in cells as determined by immunoprecipitation experiments of cells expressing REDD1 labeled with two epitope tags. While an interaction between two REDD1 molecules involving the hydrophobic pocket is unlikely to occur in vivo, this pocket may be involved in interacting with other proteins. Due to the close proximity of the hydrophobic pocket to the functional hotspot, we speculate that they together form a bipartite binding site with improved affinity for the REDD1 binding partners. Detailed analyses of the pocket show that residues at the base are conserved, but those at the ridge are not. We tested two mutations (S103L and S103W) at the edge of the pocket, which did not appreciably affect REDD1 function. However, the direct connection of this pocket with the hydrophobic core of the protein makes it difficult to effectively block it without altering the overall structure, and the functional role of this pocket requires further investigation.

Supplementary Material

Refer to Web version on PubMed Central for supplementary material.

Acknowledgments

We thank members of the Brugarolas laboratory and the Zhang laboratory for helpful discussions and Dr. Kaelin for his encouragement and helpful discussions. The content is solely the responsibility of the authors and does not represent official views from any of the granting agencies.

† This work was supported by a Fundacion Caja Madrid fellowship to S. V. and the following grants to J. B.: K08NS051843 and RO1CA129387, as well as a Basil O'Connor Starter Scholar Research Award (5-FY06-582) from the March of Dimes Foundation and a V Scholar Award from The V Foundation for Cancer Research. J. B. and X. Z. are Virginia Murchison Linthicum Scholars in Medical Research at UT Southwestern.

Abreviations

mTORC1 mammalian target of rapamycin complex 1

mLST8	mammalian lethal with Sec13 protein 8
PRAS40	proline-rich Akt substrate of 40 kDa
DEPTOR	DEP domain TOR binding protein
4E-BP1	eukaryotic initiation factor 4E (eIF4E)-binding protein 1
S6K1	S6 kinase 1
Rheb	Ras homologue enriched in brain
TSC	tuberous sclerosis complex
REDD1	regulated in development and DNA damage response 1

REFERENCES

1. Sonenberg N, Hinnebusch AG. Regulation of translation initiation in eukaryotes: mechanisms and biological targets. Cell 2009;136:731–745. [PubMed: 19239892]
2. Hara K, Maruki Y, Long X, Yoshino K, Oshiro N, Hidayat S, Tokunaga C, Avruch J, Yonezawa K. Raptor, a binding partner of target of rapamycin (TOR), mediates TOR action. Cell 2002;110:177–189. [PubMed: 12150926]
3. Kim DH, Sarbassov DD, Ali SM, King JE, Latek RR, Erdjument-Bromage H, Tempst P, Sabatini DM. mTOR interacts with raptor to form a nutrient-sensitive complex that signals to the cell growth machinery. Cell 2002;110:163–175. [PubMed: 12150925]
4. Loewith R, Jacinto E, Wullschleger S, Lorberg A, Crespo JL, Bonenfant D, Oppliger W, Jenoe P, Hall MN. Two TOR complexes, only one of which is rapamycin sensitive, have distinct roles in cell growth control. Molecular cell 2002;10:457–468. [PubMed: 12408816]
5. Kim DH, Sarbassov DD, Ali SM, Latek RR, Guntur KV, Erdjument-Bromage H, Tempst P, Sabatini DM. GbetaL, a positive regulator of the rapamycin-sensitive pathway required for the nutrient-sensitive interaction between raptor and mTOR. Molecular cell 2003;11:895–904. [PubMed: 12718876]
6. Guertin DA, Stevens DM, Thoreen CC, Burds AA, Kalaany NY, Moffat J, Brown M, Fitzgerald KJ, Sabatini DM. Ablation in mice of the mTORC components raptor, rictor, or mLST8 reveals that mTORC2 is required for signaling to Akt-FOXO and PKCalpha, but not S6K1. Developmental cell 2006;11:859–871. [PubMed: 17141160]
7. Sancak Y, Thoreen CC, Peterson TR, Lindquist RA, Kang SA, Spooner E, Carr SA, Sabatini DM. PRAS40 is an insulin-regulated inhibitor of the mTORC1 protein kinase. Molecular cell 2007;25:903–915. [PubMed: 17386266]
8. Vander Haar E, Lee SI, Bandhakavi S, Griffin TJ, Kim DH. Insulin signalling to mTOR mediated by the Akt/PKB substrate PRAS40. Nature cell biology 2007;9:316–323.
9. Peterson TR, Laplante M, Thoreen CC, Sancak Y, Kang SA, Kuehl WM, Gray NS, Sabatini DM. DEPTOR is an mTOR inhibitor frequently overexpressed in multiple myeloma cells and required for their survival. Cell 2009;137:873–886. [PubMed: 19446321]
10. Pearson RB, Dennis PB, Han JW, Williamson NA, Kozma SC, Wettenhall RE, Thomas G. The principal target of rapamycin-induced p70s6k inactivation is a novel phosphorylation site within a conserved hydrophobic domain. The EMBO journal 1995;14:5279–5287. [PubMed: 7489717]
11. Ma XM, Blenis J. Molecular mechanisms of mTOR-mediated translational control. Nature reviews 2009;10:307–318.
12. Avruch J, Long X, Ortiz-Vega S, Rapley J, Papageorgiou A, Dai N. Amino acid regulation of TOR complex 1. American journal of physiology 2009;296:E592–602. [PubMed: 18765678]
13. Long X, Lin Y, Ortiz-Vega S, Yonezawa K, Avruch J. Rheb binds and regulates the mTOR kinase. Curr Biol 2005;15:702–713. [PubMed: 15854902]

14. Manning BD, Tee AR, Logsdon MN, Blenis J, Cantley LC. Identification of the tuberous sclerosis complex-2 tumor suppressor gene product tuberin as a target of the phosphoinositide 3-kinase/akt pathway. Molecular cell 2002;10:151–162. [PubMed: 12150915]
15. Inoki K, Li Y, Zhu T, Wu J, Guan KL. TSC2 is phosphorylated and inhibited by Akt and suppresses mTOR signalling. Nature cell biology 2002;4:648–657.
16. Potter CJ, Pedraza LG, Xu T. Akt regulates growth by directly phosphorylating Tsc2. Nature cell biology 2002;4:658–665.
17. Cai SL, Tee AR, Short JD, Bergeron JM, Kim J, Shen J, Guo R, Johnson CL, Kiguchi K, Walker CL. Activity of TSC2 is inhibited by AKT-mediated phosphorylation and membrane partitioning. The Journal of cell biology 2006;173:279–289. [PubMed: 16636147]
18. Huang J, Manning BD. The TSC1-TSC2 complex: a molecular switchboard controlling cell growth. The Biochemical journal 2008;412:179–190. [PubMed: 18466115]
19. Shoshani T, Faerman A, Mett I, Zelin E, Tenne T, Gorodin S, Moshel Y, Elbaz S, Budanov A, Chajut A, Kalinski H, Kamer I, Rozen A, Mor O, Keshet E, Leshkowitz D, Einat P, Skaliter R, Feinstein E. Identification of a novel hypoxia-inducible factor 1-responsive gene, RTP801, involved in apoptosis. Molecular and cellular biology 2002;22:2283–2293. [PubMed: 11884613]
20. Brugarolas J, Lei K, Hurley RL, Manning BD, Reiling JH, Hafen E, Witters LA, Ellisen LW, Kaelin WG Jr. Regulation of mTOR function in response to hypoxia by REDD1 and the TSC1/TSC2 tumor suppressor complex. Genes & development 2004;18:2893–2904. [PubMed: 15545625]
21. Brugarolas, J. mTOR signaling and hypoxia. In: PJ, P. V. a. H., editor. mTOR Pathway and mTOR inhibitors in Cancer Therapy. Humana Press; 2009.
22. Wang Z, Malone MH, Thomenius MJ, Zhong F, Xu F, Distelhorst CW. Dexamethasone-induced gene 2 (dig2) is a novel pro-survival stress gene induced rapidly by diverse apoptotic signals. The Journal of biological chemistry 2003;278:27053–27058. [PubMed: 12736248]
23. Ellisen LW, Ramsayer KD, Johannessen CM, Yang A, Beppu H, Minda K, Oliner JD, McKeon F, Haber DA. REDD1, a developmentally regulated transcriptional target of p63 and p53, links p63 to regulation of reactive oxygen species. Molecular cell 2002;10:995–1005. [PubMed: 12453409]
24. Corradetti MN, Inoki K, Guan KL. The stress-inducted proteins RTP801 and RTP801L are negative regulators of the mammalian target of rapamycin pathway. The Journal of biological chemistry 2005;280:9769–9772. [PubMed: 15632201]
25. Liu L, Cash TP, Jones RG, Keith B, Thompson CB, Simon MC. Hypoxia-induced energy stress regulates mRNA translation and cell growth. Molecular cell 2006;21:521–531. [PubMed: 16483933]
26. DeYoung MP, Horak P, Sofer A, Sgroi D, Ellisen LW. Hypoxia regulates TSC1/2-mTOR signaling and tumor suppression through REDD1-mediated 14-3-3 shuttling. Genes & development 2008;22:239–251. [PubMed: 18198340]
27. Sofer A, Lei K, Johannessen CM, Ellisen LW. Regulation of mTOR and cell growth in response to energy stress by REDD1. Molecular and cellular biology 2005;25:5834–5845. [PubMed: 15988001]
28. Van Duyne GD, Standaert RF, Karplus PA, Schreiber SL, Clardy J. Atomic structures of the human immunophilin FKBP-12 complexes with FK506 and rapamycin. Journal of molecular biology 1993;229:105–124. [PubMed: 7678431]
29. Adams PD, Grosse-Kunstleve RW, Hung LW, Ioerger TR, McCoy AJ, Moriarty NW, Read RJ, Sacchettini JC, Sauter NK, Terwilliger TC. PHENIX: building new software for automated crystallographic structure determination. Acta crystallographica 2002;58:1948–1954.
30. Emsley P, Cowtan K. Coot: model-building tools for molecular graphics. Acta crystallographica 2004;60:2126–2132.
31. Thompson JD, Gibson TJ, Plewniak F, Jeanmougin F, Higgins DG. The CLUSTAL_X windows interface: flexible strategies for multiple sequence alignment aided by quality analysis tools. Nucleic acids research 1997;25:4876–4882. [PubMed: 9396791]
32. Altschul SF, Madden TL, Schaffer AA, Zhang J, Zhang Z, Miller W, Lipman DJ. Gapped BLAST and PSI-BLAST: a new generation of protein database search programs. Nucleic acids research 1997;25:3389–3402. [PubMed: 9254694]

33. Pei J, Kim BH, Grishin NV. PROMALS3D: a tool for multiple protein sequence and structure alignments. Nucleic acids research 2008;36:2295–2300. [PubMed: 18287115]
34. Jones DT, Taylor WR, Thornton JM. The rapid generation of mutation data matrices from protein sequences. Comput Appl Biosci 1992;8:275–282. [PubMed: 1633570]
35. Adachi, J.; Hasegawa, M. Computer Science Monographs. Institute of Statistical Mathematics; Tokyo: 1992. Molphy: Programs for Molecular Phylogenetics Based on Maximum Likelihood..
36. Saitou N, Nei M. The neighbor-joining method: a new method for reconstructing phylogenetic trees. Molecular biology and evolution 1987;4:406–425. [PubMed: 3447015]
37. Kishino H, Miyata T, Hasegawa M. Maximum likelihood inference of protein phylogeny and the origin of chloroplasts. J Mol Evol 1990;30:10.
38. Wilson IA, Haft DH, Getzoff ED, Tainer JA, Lerner RA, Brenner S. Identical short peptide sequences in unrelated proteins can have different conformations: a testing ground for theories of immune recognition. Proceedings of the National Academy of Sciences of the United States of America 1985;82:5255–5259. [PubMed: 2410917]
39. Reiling JH, Hafen E. The hypoxia-induced paralogs Scylla and Charybdis inhibit growth by down-regulating S6K activity upstream of TSC in Drosophila. Genes & development 2004;18:2879–2892. [PubMed: 15545626]
40. Hutchinson EG, Thornton JM. PROMOTIF--a program to identify and analyze structural motifs in proteins. Protein Sci 1996;5:212–220. [PubMed: 8745398]
41. Holm L, Kaariainen S, Rosenstrom P, Schenkel A. Searching protein structure databases with DaliLite v.3. Bioinformatics (Oxford, England) 2008;24:2780–2781.
42. Shi S, Zhong Y, Majumdar I, Sri Krishna S, Grishin NV. Searching for three-dimensional secondary structural patterns in proteins with ProSMoS. Bioinformatics (Oxford, England) 2007;23:1331–1338.
43. Murzin AG, Brenner SE, Hubbard T, Chothia C. SCOP: a structural classification of proteins database for the investigation of sequences and structures. Journal of molecular biology 1995;247:536–540. [PubMed: 7723011]
44. Yang X, Lee WH, Sobott F, Papagrigoriou E, Robinson CV, Grossmann JG, Sundstrom M, Doyle DA, Elkins JM. Structural basis for protein-protein interactions in the 14-3-3 protein family. Proceedings of the National Academy of Sciences of the United States of America 2006;103:17237–17242. [PubMed: 17085597]
45. Bridges D, Moorhead GB. 14-3-3 proteins: a number of functions for a numbered protein. Sci STKE 2005;2005:re10. [PubMed: 16091624]
46. Yaffe MB, Rittinger K, Volinia S, Caron PR, Aitken A, Leffers H, Gamblin SJ, Smerdon SJ, Cantley LC. The structural basis for 14-3-3:phosphopeptide binding specificity. Cell 1997;91:961–971. [PubMed: 9428519]
47. Kovacina KS, Park GY, Bae SS, Guzzetta AW, Schaefer E, Birnbaum MJ, Roth RA. Identification of a proline-rich Akt substrate as a 14-3-3 binding partner. The Journal of biological chemistry 2003;278:10189–10194. [PubMed: 12524439]
48. Brunet A, Bonni A, Zigmond MJ, Lin MZ, Juo P, Hu LS, Anderson MJ, Arden KC, Blenis J, Greenberg ME. Akt promotes cell survival by phosphorylating and inhibiting a Forkhead transcription factor. Cell 1999;96:857–868. [PubMed: 10102273]
49. Tzivion G, Avruch J. 14-3-3 proteins: active cofactors in cellular regulation by serine/threonine phosphorylation. The Journal of biological chemistry 2002;277:3061–3064. [PubMed: 11709560]

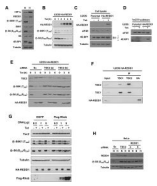

FIGURE 1.

REDD1 is both necessary and sufficient for hypoxia-induced mTORC1 inhibition. (**A**) Immunoblot analysis of HeLa cells in normoxia (N) or hypoxia (H). (**B**) Western blot analyses of U2OS HA-REDD1-inducible cells treated with tetracycline (Tet) for the indicated number of hours. Western blot analyses (**C**) and m^7GTP pulldown assays (**D**) of U2OS HA-REDD1-inducible cells (or parental U2OS cells as a control). (**E**) Western blot of HeLa cells transfected with the stated siRNA oligos and exposed to normoxia (N) or hypoxia (H). (**F**) Immunoprecipitation analysis of TSC1/TSC2 binding to REDD1 in U2OS HA-REDD1-inducible cells treated with tetracycline (**G**) Western blot of U2OS HA-REDD1 cells transfected with the indicated amounts of *Flag-Rheb* (or *EGFP* as a control) induced (or not) with tetracycline (Tet). (**H**) Western blot of HeLa cells transfected with the indicated siRNA oligos and exposed to normoxia (N) or hypoxia (H).

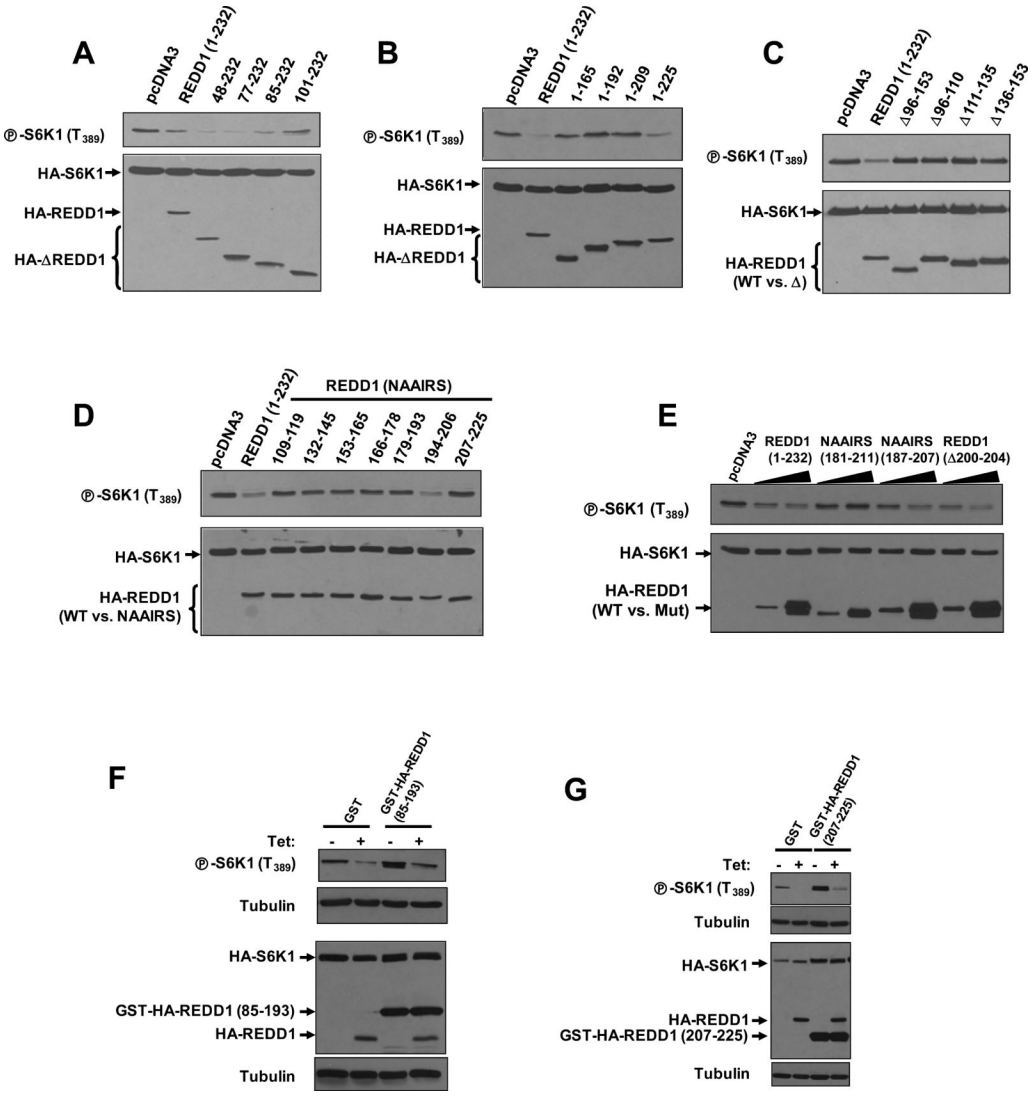

FIGURE 2.

Deletion/substitution analyses identify two regions in REDD1 required for mTORC1 inhibition, which do not function as dominant negative. Western blot analyses of HeLa cells transfected with expression vectors for *HA-S6K1* and various *HA-REDD1* mutants: (**A**) N-terminal deletions, (**B**) C-terminal deletions, (**C**) internal deletions and (**D, E**) substitutions with a flexible linker (NAAIRS [single letter amino acid code]) Western blot analyses of U2OS HA-REDD1-inducible cells transfected with *HA-S6K1* along with either *GST-HA-REDD1*$^{85\text{-}193}$ (**F**) or *GST-HA-REDD1*$^{207\text{-}225}$ (**G**) using *GST* as a control, and induced (or not) with tetracycline (Tet) to express HA-REDD1.

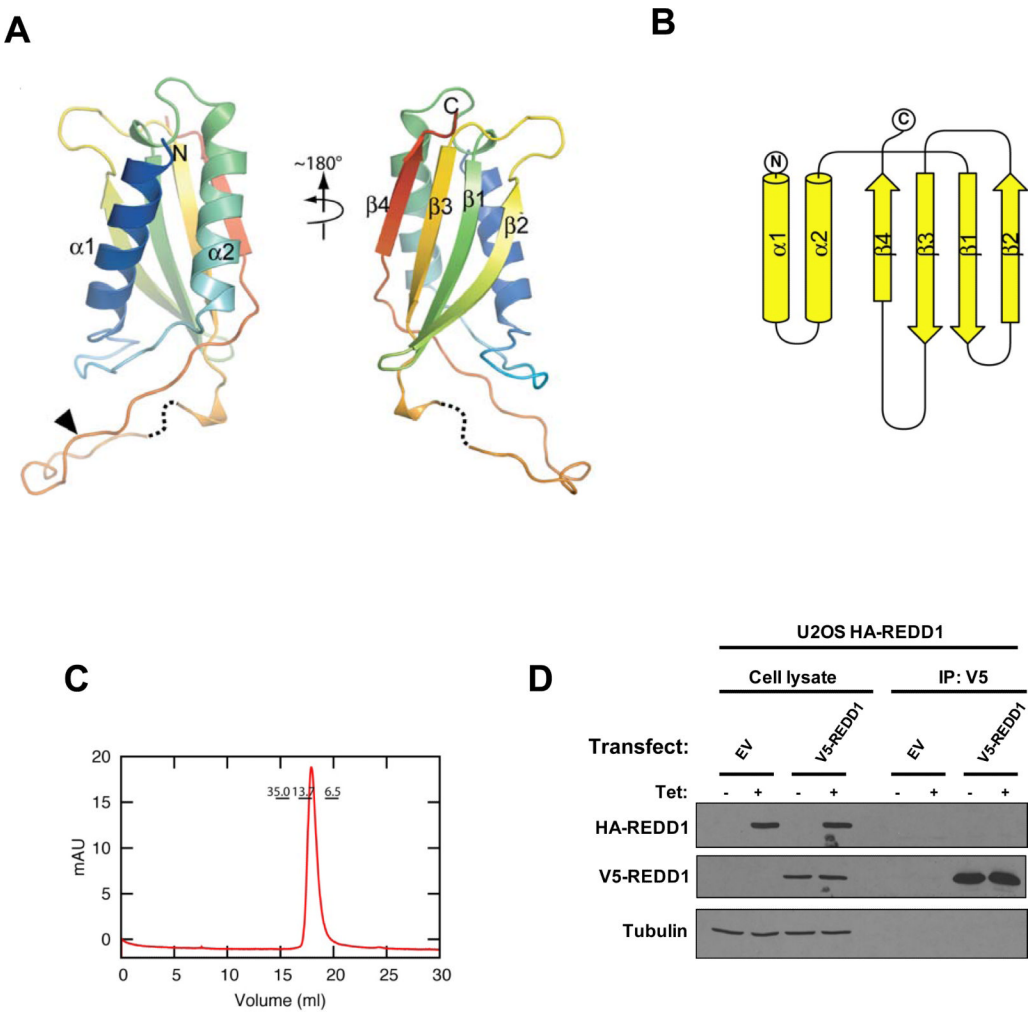

FIGURE 3.

REDD1 exhibits a novel topology and does not oligomerize. (**A**) Cartoon representation of the REDD1$^{89\text{-}226\Delta\phi}$ structure colored in rainbow mode from the N- to the C-terminus. The dotted line represents disordered region. The black arrowhead indicates the location of the ^{200}FLPGF^{204} deletion. (**B**) Diagram of REDD1 topology. (**C**) Gel filtration chromatography of purified REDD1$^{89\text{-}226\Delta\phi}$ (elution positions of molecular weight standards indicated). (**D**) Western blot analyses of anti-V5 immunoprecipitates (or inputs) from U2OS HA-REDD1-inducible cells transfected with *V5-REDD1* (or empty vector, EV) and induced (or not) with tetracycline (Tet).

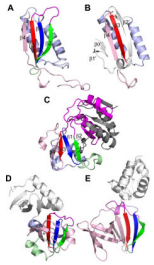

FIGURE 4.

Closest structural relatives of REDD1 exhibit markedly different topologies. (**A**) Ribbon model of $^{REDD189\text{-}226\Delta\phi}$ (strands labeled numerically from N- to C-terminus [β1-β4] including connecting psi-loop formed by β1-β3). (**B**) Ribbon structure of the top dali hit (ID: 1i2l) (strand order [2'3401'] based on strands β3 and β4 corresponding to REDD1). (**C**) Ribbon structure of top ProSMoS hit, the YrdC-like hypothetical protein (PDB ID: 1K7J) with YrdC/RibA fold core depicted in gray. Ribbon structures of ProSMoS-identified psi-loops in a pua domain-like structure (PDB ID: 3d79; **D**) and a lexA-like family structure (PDB ID: 2fjr; **E**). In structures B-E, secondary structural elements (β strands and connecting psi-loop) corresponding to those present in REDD1 are similarly colored; unrelated structures are colored in white or gray.

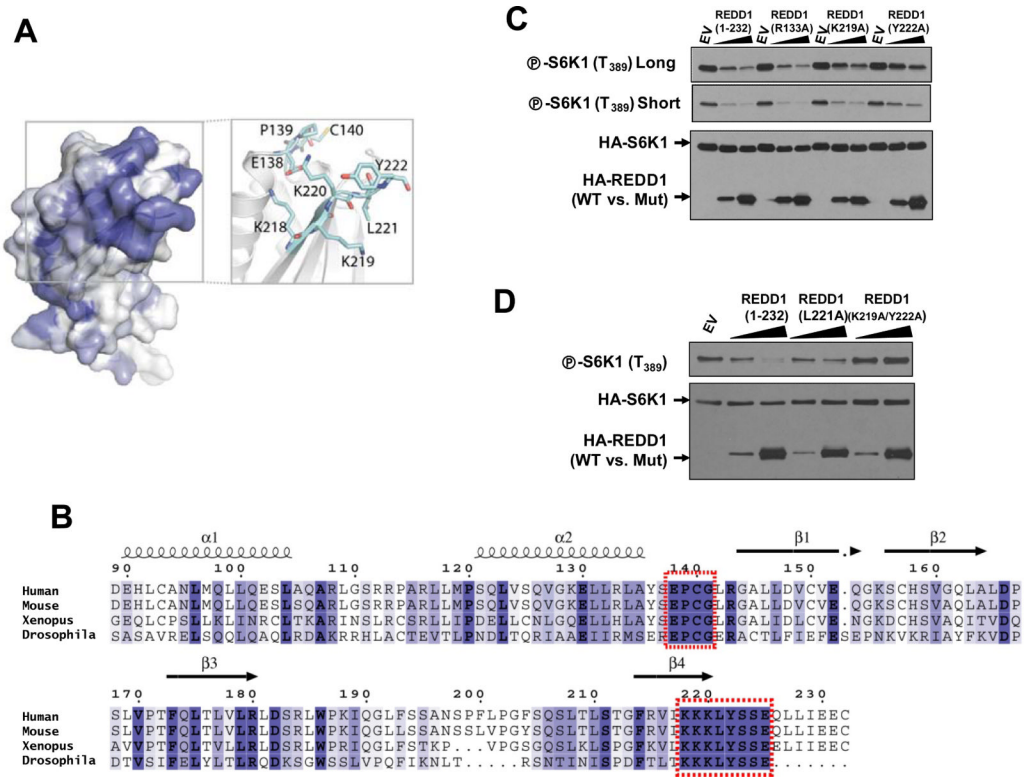

FIGURE 5.

Conservation mapping onto REDD1 protein surface and mutagenesis studies reveal a functionally important hotspot. (**A**) Conservation mapping of REDD1 surface using an increasing blue color gradient proportional to the degree of conservation and inlet stick representation of conserved residues. (**B**) Sequence alignment of REDD1 from different species with blue color gradient signifying conservation (as in A) and red boxes demarcating the two stretches of sequence forming the conserved surface patch. (**C, D**) Functional evaluation of residues involved in conserved surface patch by mutagenesis and western blot analyses in HeLa cells transfected with *HA-S6K1* (EV, empty vector).

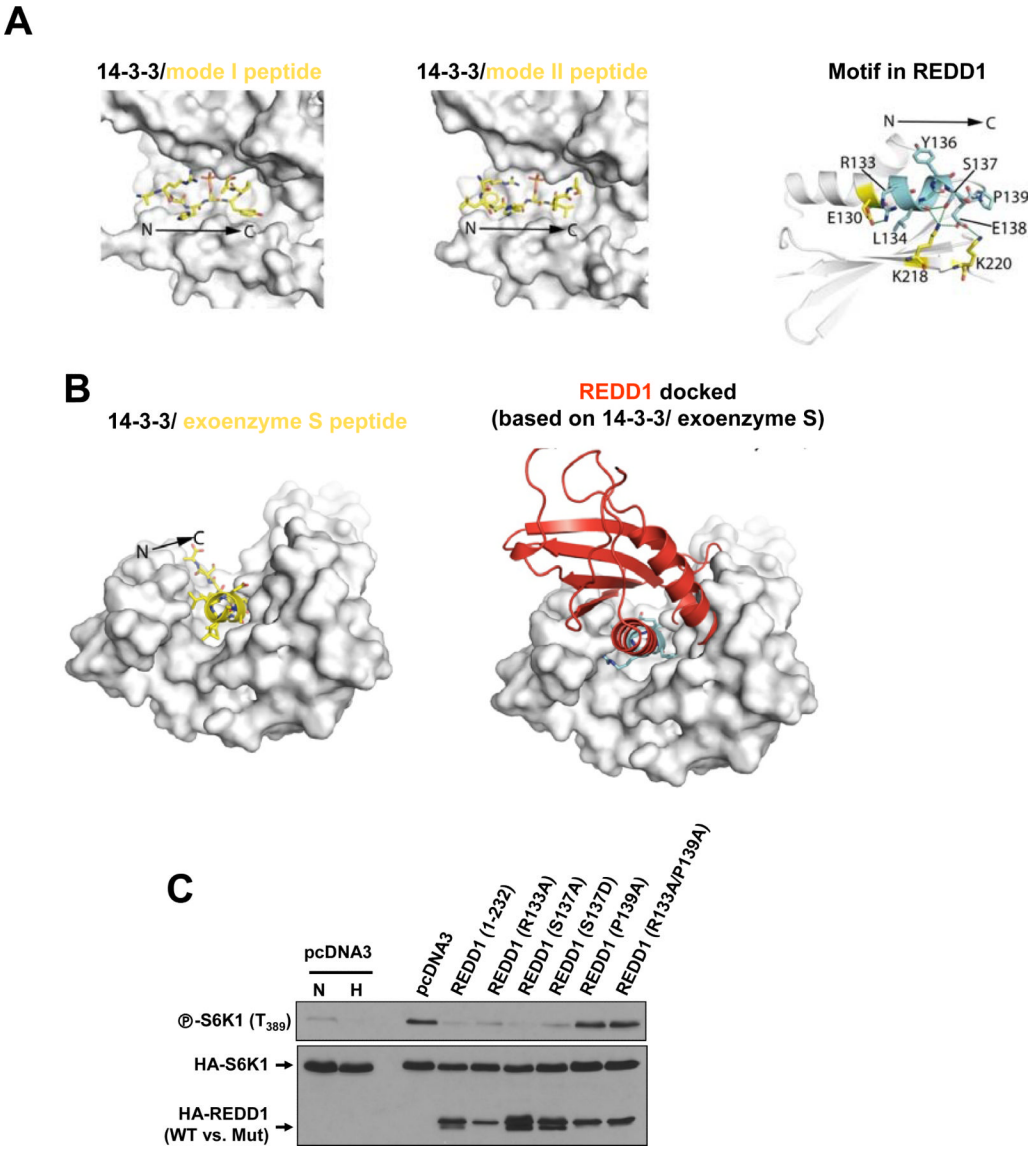

FIGURE 6.

Structure-based docking studies of REDD1 binding to 14-3-3. (**A**) Illustration of peptides (yellow) in 14-3-3ζ binding mode I (PDB ID: 1QJB) and II (PDB ID: 1QJA) compared to the putative 14-3-3 binding motif in REDD1. (**B**) Depiction of unusual exoenzyme S binding to 14-3-3β (PDB ID: 2C23) and docking of REDD1$^{89\text{-}226\Delta\phi}$ based on this binding mode showing multiple steric clashes. (**C**) Functional evaluation of putative 14-3-3-binding site by mutagenesis and western blot analyses in HeLa cells transfected with *HA-S6K1* (*pcDNA3* transfected HeLa cells exposed to either normoxia [N] or hypoxia [H] are shown as a control).

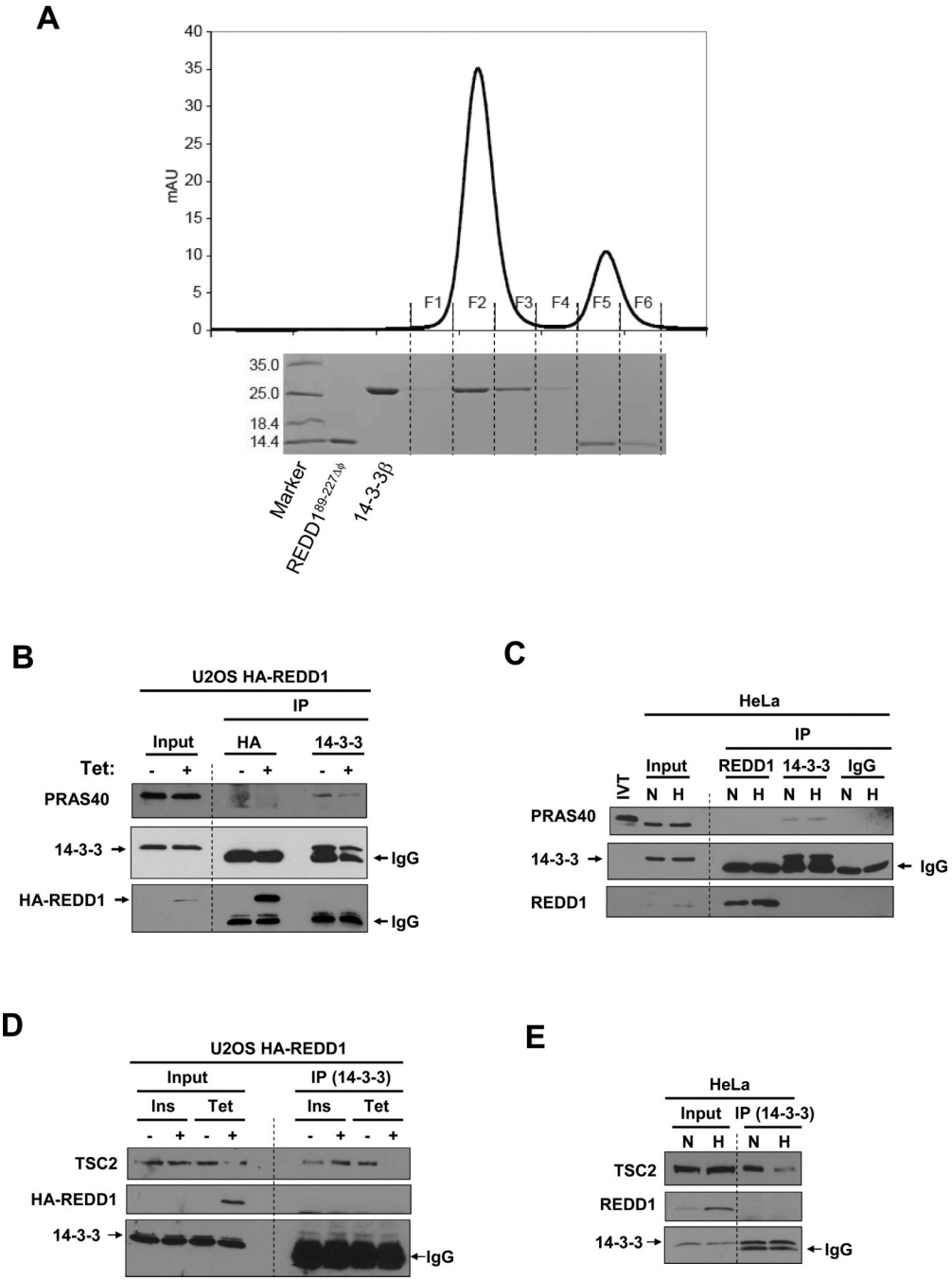

FIGURE 7.

REDD1 does not interact with 14-3-3 proteins in vitro or in vivo. (**A**) Elution profile of the recombinant REDD1$^{89\text{-}226\Delta\phi}$ and 14-3-3β mix and Coomasie stained SDS-PAGE analyses from corresponding fractions; purified REDD1$^{89\text{-}226\Delta\phi}$ and 14-3-3β shown as controls. (**B**) Immunoprecipitation studies of both 14-3-3 and HA-REDD1 in U2OS HA-REDD1-inducible cells induced (or not) to express REDD1. (**C**) Immunoprecipitation analysis of both 14-3-3 and endogenous REDD1 in HeLa cells in which REDD1 is induced by hypoxia (H), or not (normoxia, N); in vitro translated Flag-PRAS40 [IVT] is shown as a control. TSC2 binding to 14-3-3 analysis in (**D**) U2OS HA-REDD1-inducible cells treated (or not)

with insulin (Ins) or Tetracycline (Tet) and (**E**) HeLa cells exposed to normoxia (N) or hypoxia (H).

TABLE 1

Data collection and refinement statistics

Data collection parameters		
Dataset	1 (Seleno-Met SAD)	2
Space group	P1	P1
Unit cell (Å, °)	a=33.2, b=36.8, c=47.8, α=77.6, β=89.1, γ=86.3	a=33.3, b=36.6, c=48.0, α=77.6, β=89.1, γ=86.2
Wavelength (Å)	0.97926	1.2829
Resolution (Å)	50-2.2(2.28-2.2)[a]	50-2.00(2.07-2.00)
Number of reflections	55284	56986
Number of unique reflections	11682	14319
Completeness (%)	96.0 (87.2)	95.9 (94.0)
I/σ	23.6 (5.5)	25.3 (9.1)
R_{sym} (%)[b]	7.9 (23.2)	6.8 (25.9)
Refinement parameters		
R_{work}/R_{free} (%)		17.7 /21.4
Molecules/asymmetric unit		2
Number of protein atoms		1921
Number of solvent atoms		203
rmsd bond length (Å)		0.003
rmsd bond angle (°)		0.770
Ramachandran plot (favored, allowed, disallowed)(%)		90.8, 9.2, 0

[a] Numbers in parenthesis refer to the highest resolution shell.

[b] $R_{sym} = \Sigma|I-\langle I\rangle|/\Sigma I$, where I is the observed intensity of a reflection, and <I> is the average intensity of all the symmetry related reflections.